CrossMark
click for updates

Stable ambipolar organic–inorganic heterojunction field-effect transistors and inverters with Cytop interlayer†

Sheng Sun, Linfeng Lan,* Yuzhi Li, Honglong Ning, Rihui Yao, Lei Wang and Junbiao Peng

In this study, ambipolar field-effect transistors (FETs) based on organic–inorganic bilayer structures were investigated. InO_x and pentacene were selected as n-type and p-type semiconductors, respectively. To improve the hole mobility, poly(perfluorobutenylvinylether) (Cytop) layer was introduced to modify the surface of InO_x. The ambipolar FETs showed hole and electron mobilities of 1.1 and 0.1 $cm^2 V^{-1} s^{-1}$, respectively and excellent electrical stability under gate bias stress. Furthermore we found that ambipolar FETs could be integrated into functional complementary metal oxide semiconductor (CMOS)-like inverters and exhibited high peak gain (>50). This work provides a general method for realizing ambipolar FETs based on organic–inorganic hybrid structure.

Introduction

In recent years, ambipolar field-effect transistors (FETs) have been extensively studied for technological applications in complementary logic circuits due to their unique operation, which allows both holes and electrons to be injected and transported depending on the gate bias in a single device.[1–5] Organic semiconductors and metal-oxide semiconductors are two families of active materials that are currently drawing much attention in FETs.[6–8] However, they usually exhibit unipolar charge transport, which limits their applications in ambipolar FETs. Although organic semiconductors can transport both holes and electrons at the same time, the electron transport for most of the organic semiconductor is poor compared to the hole transport.[9] In contrary to the organic semiconductors, most metal-oxide semiconductors have only n-type characteristics.[10,11] Therefore, it is possible to achieve ambipolar transport by using organic semiconductor/oxide semiconductor bilayer structure. Nakanotani *et al.* developed an ambipolar FET based on an organic–inorganic hybrid structure containing indium zinc oxide and pentacene bilayer with hole and electron mobilities of 0.14 and 13.8 $cm^2 V^{-1} s^{-1}$, respectively.[12] This work opened up a new field in ambipolar FETs fabrication. Smith *et al.* reported an air-stable solution-processed hybrid transistors with hole and electron mobilities exceeding 2 $cm^2 V^{-1} s^{-1}$, but the device showed ambipolar performance only in the dual-

gated model, which is complicated and costly.[13] Yang *et al.* reported ambipolar FETs based on pentacene/ZnO hybrid structures and got balance hole and electron mobilities of 0.34 and 0.38 $cm^2 V^{-1} s^{-1}$ respectively.[14] Kim *et al.* reported ambipolar FETs based on carbon nanotube/zinc tin oxide heterostructures by inkjet printing with hole and electron mobilities exceeding 2 $cm^2 V^{-1} s^{-1}$, but the processing temperature is as high as 500 °C, which was too high to fabricate on most of the flexible substrates.[15] Ambipolar FETs have also been realized by several approaches, such as bilayer and blend. But most work can't exhibit good stability.[16–20]

Herein, we report on a high-stable ambipolar FET based on an organic–inorganic bilayer structure channel. For the p-type organic semiconductor, we chose pentacene which was well studied and exhibit stable performance. InO_x was selected as the n-type metal oxide semiconductor. In our previous work, directly patternable solution-processed InO_x films could be fabricated with an economic and environmentally friendly approach at low temperature.[21] To improve the p-type performance, the surface of the InO_x layer was modified by Cytop.[22]

Experimental section

Fig. 1 shows the schematic structure of the ambipolar FET. Firstly, a 300 nm thick Al–Nd (3 wt%) film was deposited with DC sputtering and patterned with conventional photolithography method. Afterwards, Al:Nd film was anodized for 1.5 h to produce a layer of 200 nm thick AlO_x:Nd (41 nF cm^{-2}) on the surface of the Al:Nd film as the gate insulator. After 5 min oxygen plasma treatment, the InO_x film was spin-coated and patterned in a facile method, following which the InO_x film underwent an annealing process at 220 °C for 2 h in air. After

State Key Laboratory of Luminescent Materials and Devices (South China University of Technology), Wushan Road 381#, Tianhe District, Guangzhou, China. E-mail: lanlinfeng@scut.edu.cn
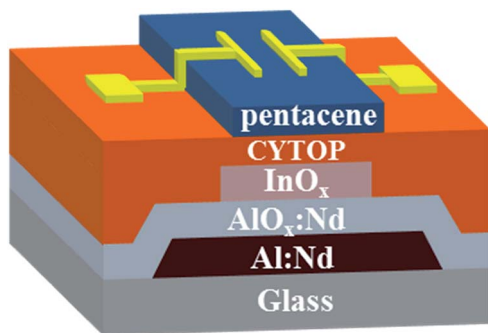
Fig. 1 Schematic diagram of ambipolar FETs based on InO_x/Cytop/pentacene hybrid structure.

that, the 45 nm thick Cytop film was spin-coated as an interlayer to modify the growth of pentacene. After that, a layer of 30 nm thick pentacene film was thermally evaporated onto the insulator at room temperature under a vacuum pressure of $\sim3 \times 10^{-4}$ Pa with a deposition rate of 0.1 Å s^{-1}. Then a 45 nm thick Au film was thermally evaporated onto the pentacene film through a shadow mask, defining a channel width/length (W/L) of 500/70 μm. The TFT characterizations were measured with a semiconductor parameter analyzer (Agilent 4155C) and a probe station at room temperature (RT) in vacuum environment.

Results and discussion

Fig. 2 shows the output and transfer characteristics of the ambipolar FETs based on the organic–inorganic heterostructures with the Cytop layer. The FETs exhibited ambipolar performance with hole and electron mobilities of 1.1 and 0.1 cm^2 V^{-1} s^{-1}, respectively, which were extracted from the following equation,

$$I_{DS} = \mu \frac{W}{2L} C_i (V_G - V_T)^2, \tag{1}$$

where I_{DS} is drain-source current, V_G is gate voltage, V_T is the threshold voltage, C_i is capacitance density. Specifically, C_i (22 nF cm^{-2}) for hole mobility and C_i (41 nF cm^{-2}) for electron mobility were different, because the 20 nm thick InO_x and 45 nm thick Cytop layer were acted as the dielectric layers when the FET was operated in the p-channel mode, as shown in Fig. 3. C_i for hole mobility was constant as gate voltage varies from 0 V to −30 V, as shown in Fig. S3.†

It could be also seen from Fig. 2 the hysteresis between the forward and reverse sweeps in the transfer curve is too little to be detected. It implies that the amount of fast traps in the bulk or at the interface is small. It is worth noting that the ambipolar FETs without Cytop or with 20 nm Cytop exhibited large hysteresis, as shown in Fig. S1,† which was attributed to the large amount of hole traps on the surface of InO_x (and 20 nm Cytop was not thick enough to block the holes from trapping into InO_x). Besides Cytop, polymethyl methacrylate (PMMA) and polystyrene (PS) were also employed as the modification layer. It can be seen from Fig. S2† that the PMMA and PS layer can also improve FET performance, but not as good as Cytop.[23,24] Compared to PMMA and PS, Cytop film is smoother and more hydrophobic. Besides, the density of states (DOS) of Cytop film is low due to the low dielectric constant, resulting in higher mobility and better stability.

Fig. 4(a) and (b) show the atomic force microscopy (AFM) images of pentacene films on InO_x and Cytop/InO_x, respectively. The pentacene grain size on InO_x was much larger than that on Cytop/InO_x. The grain size was based on surface roughness and surface energy. It is known that the pentacene film tends to grow into larger size on the surface of low roughness and high surface energy.[25] The roughness of InO_x (1.2 nm) is similar as that of Cytop (1.4 nm), tested by AFM. The surface energy of InO_x (45.6 mN m^{-1}) is larger than that of Cytop (13.5 mN m^{-1}), which was calculated by OWRK (Owens–Wendt–Rabel–Kaelbe) equation using contact angles of water, ethylene glycol and diiodomethane on the surface of InO_x and Cytop.[26,27] Although the pentacene grain size on InO_x is larger than that on Cytop/InO_x, the hole transport of the FETs without Cytop can hardly be
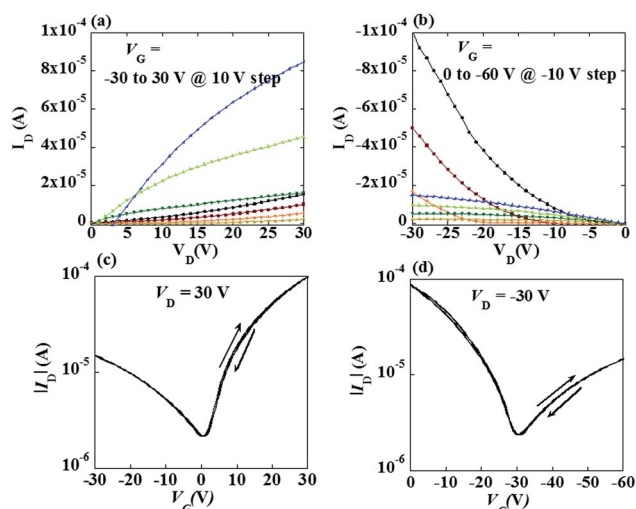

Fig. 2 Output characteristics of ambipolar FETs based on InO_x/Cytop/pentacene hybrid structure: (a) in electron enhancement mode and (b) in electron enhancement mode. Transfer characteristics of ambipolar FETs based on InO_x/Cytop/pentacene hybrid structure: (c) $V_D = 30$ V and (d) $V_D = -30$ V. Every curve includes forward and reverse sweeps.
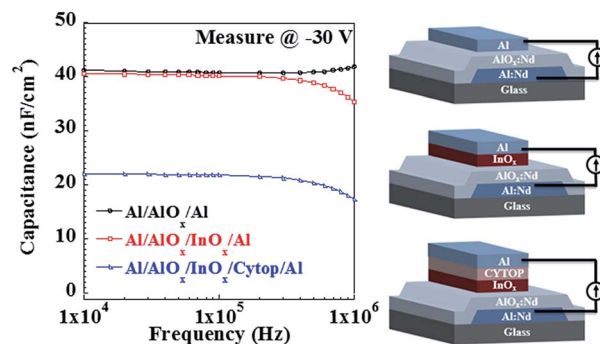

Fig. 3 Capacitance vs. frequency plots measured at −30 V for AlO_x:Nd, AlO_x:Nd/InO_x and AlO_x:Nd/InO_x/Cytop; inset: the structures of these three capacitances.
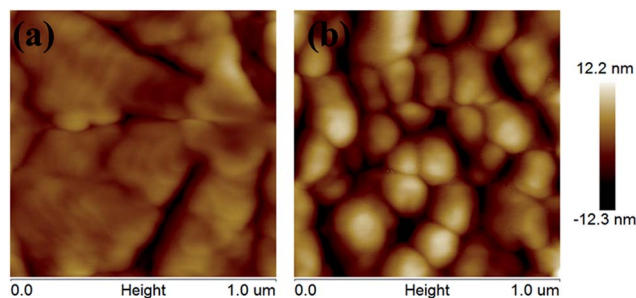
Fig. 4 AFM images of pentacene films on (a) InO_x, and (b) Cytop/InO_x.

Fig. 6 The time-dependent transfer property ((a) $V_D = 30$ V and (b) $V_D = -30$ V) under negative gate-bias-stress for ambipolar FETs stress condition: $V_G = -30$ V, $V_D = -30$ V. Every curve includes forward and reverse sweeps.

Fig. 7 (a) The voltage transfer characteristics of the CMOS-like inverter at different supply voltages of 30 V, 40 V, 50 V. Inset: the circuit diagram of the inverter. (b) The corresponding voltage gains of the inverter.

detected. This phenomenon was ascribed to the high electron density of InO_x. In FETs without Cytop, the large amount of the undepleted electrons can act as the hole traps, so the holes in the organic semiconductor are trapped. After inserted with a Cytop interlayer, the undepleted electrons from InO_x are blocked by Cytop, so the holes in pentacene cannot be trapped by the electrons from InO_x. As a result, the hole transport of the FETs with Cytop layer improves.

The electrical stability under gate bias stress is an important parameter in FETs. Fig. 5 and 6 show negative bias stress (NBS) and positive bias stress (PBS) stability of the ambipolar FETs, respectively. Almost no threshold voltage shift was found during the PBS test, while a little positive shift was found during the NBS test. The high bias stability was ascribed to the Cytop modification layer. For electron transport, the Cytop acted as the passivation layers to prevent the back channel of InO_x from interacting with oxygen and moisture from the air. For hole transport, the Cytop layer can passivated the OH groups on the InO_x surface. It is known that the OH groups at the insulator/semiconductor interface would cause device instability. There are no OH groups in the Cytop molecule, and the Cytop films are highly hydrophobic with a water contact angle of $106°$ which is better than those of many other polymers. Thus, the Cytop modification will improve the electrical stability for both electron and hole transport.[22]

Finally, a complementary-like inverter was fabricated with the integration of two identical pentacene/Cytop/InO_x ambipolar FETs. Fig. 7(a) shows the voltage transfer characteristics. The input voltage was applied through the Al:Nd bottom gate
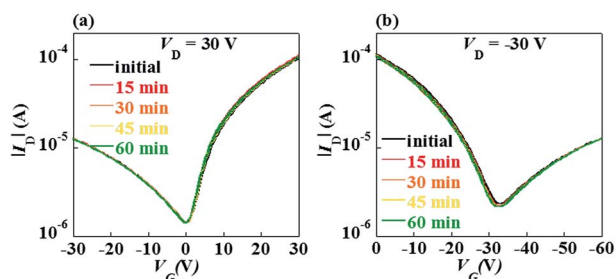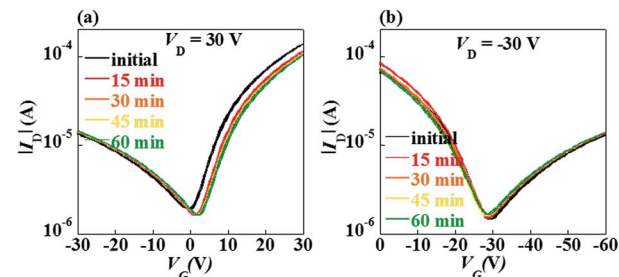
electron. Three supply voltages (V_{DD}) of 30 V, 40 V and 50 V were biased to the inverter respectively. The output voltage (V_{OUT}) varied from high to low in response to the swing of the V_{IN} from low to high, and sharp inversions were found to be near 5 V, 10 V and 15 V, respectively. The voltage grain, defined as $|dV_{OUT}/dV_{IN}|$ was calculated from the voltage transfer curves, as shown in Fig. 7(b). The voltage gains reached maximum value of 40, 54 and 58. The V_{OUT} was not constant at both high and low values of V_{IN}, where V_{OUT} increased slightly with V_{IN}. This common feature of ambipolar inverters arose because one of the ambipolar FETs is not completely turned off while the second FET was turned on.[15] Overall, the inverter exhibited better electrical stability and voltage gain compared to most of other inverters based on unipolar p-type and n-type FETs and ambipolar FETs.[28–30]

Conclusions

In conclusion, the stable ambipolar FETs and CMOS-like inverters based on organic–inorganic heterostructures were fabricated. Pentacene and InO_x as the semiconducting p-type and n-type layers composed the hybrid structure. Cytop was inserted to modify the organic–inorganic interface by reducing the surface energy to improve the hole mobility and the stability. As a result the ambipolar FETs showed hole and electron mobilities of 1.1 and 0.1 cm^2 V^{-1} s^{-1}, respectively and excellent electrical stability under gate bias stress. COMS-like

Fig. 5 The time-dependent transfer property ((a) $V_D = 30$ V and (b) $V_D = -30$ V) under negative gate-bias-stress for ambipolar FETs stress condition: $V_G = 30$ V, $V_D = 30$ V. Every curve includes forward and reverse sweeps.
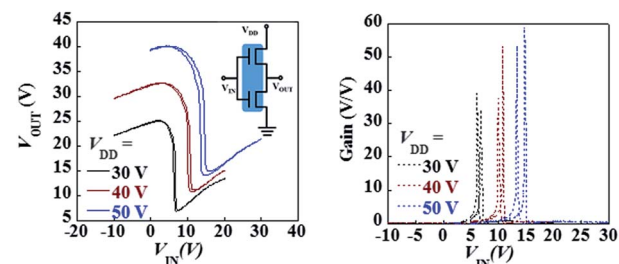
inverters showed clear signal inverting operation with a high gain of 58. These results suggest that FETs based on organic–inorganic heterostructures are promising candidates for realizing high stable ambipolar logic devices.

Notes and references

1 A. Dodabalapur, H. E. Katz, L. Torsi and R. C. Haddon, *Science*, 1995, **269**, 1560.
2 J. Zaumseil and H. Sirringhaus, *Appl. Phys. Lett.*, 2007, **107**, 1296.
3 B. B. Y. Hsu, E. B. Namdas, J. D. Yuen, S. Cho, I. D. W. Samuel and A. J. Heeger, *Adv. Mater.*, 2010, **24**, 4649.
4 Y. Zhao, Y. Guo and Y. Liu, *Adv. Mater.*, 2013, **25**, 5372.
5 S. Watanabe, T. Fujita, J. Ribierre, K. Takaishi, T. Muto, C. Adachi, M. Uchiyama, T. Aoyama and M. Matsumoto, *ACS Appl. Mater. Interfaces*, 2016, **8**, 17574.
6 H. Sirringhaus, *Adv. Mater.*, 2014, **26**, 1319.
7 B. Kumar, B. K. Kaushik and Y. S. Negi, *Polym. Rev.*, 2014, **54**, 3.
8 E. Fortunato, P. Barquinha and R. Martins, *Adv. Mater.*, 2012, **24**, 2945.
9 Y. Zhao, Y. Guo and Y. Liu, *Adv. Mater.*, 2013, **25**, 5372.
10 K. Nomura, T. Kamiya, H. Ohta, T. Uruga, M. Hirano and H. Hosono, *Phys. Rev. B: Condens. Matter Mater. Phys.*, 2007, **75**, 035212.
11 L. Lan, N. Xiong, P. Xiao, M. Li, H. Xu, R. Yao, S. Wen and J. Peng, *Appl. Phys. Lett.*, 2013, **102**, 242102.
12 H. Nakanotani, M. Yahiro, C. Adachi and K. Yano, *Appl. Phys. Lett.*, 2007, **90**, 262104.
13 J. Smith, A. Bashir, G. Adamopoulos, J. E. Anthony, D. D. C. Bradley, R. Hamilton, M. Heeney, I. McCulloch and T. D. Anthopoulos, *Adv. Mater.*, 2010, **22**, 3598.
14 C. Yang, Y. Kwack, S. H. Kim, T. K. An, K. Hong, S. Nam, M. Park, W. Choi and C. E. Park, *Org. Electron.*, 2011, **12**, 411.
15 B. Kim, S. Jang, M. L. Geier, P. L. Prabhumirashi, M. C. Hersam and A. Dodabalapur, *Appl. Phys. Lett.*, 2014, **104**, 62101.
16 J. Shi, H. Wang, D. Song, H. Tian, Y. Geng and D. Yan, *Adv. Funct. Mater.*, 2007, **17**, 397.
17 E. J. Meijer, D. M. Deleeuw, S. Setayesh, E. V. Veenendaal, B. H. Huisman, P. W. Blom, J. C. Hummelen, U. Scherf and T. M. Klapwijk, *Nat. Mater.*, 2003, **2**, 678.
18 K. Baeg, D. Khim, S. Jung, M. Kang, I. You, D. Kim, A. Facchetti and Y. Noh, *Adv. Mater.*, 2012, **24**, 5433.
19 I. Meager, M. Nikolka, B. C. Schroeder, C. B. Nielsen, M. Planells, H. Bronstein, J. W. Rumer, D. I. James, R. S. Ashraf, A. Sadhanala, P. Hayoz, J. Flores, H. Sirringhaus and I. McCulloch, *Adv. Funct. Mater.*, 2014, **24**, 7109.
20 J. Y. Choi, W. Kang, B. Kang, W. Cha, S. K. Son, Y. Yoon, H. Kim, Y. Kang, M. J. Ko, H. J. Son, K. Cho, H. J. Cho and B. Kim, *ACS Appl. Mater. Interfaces*, 2015, **7**, 6002.
21 Y. Li, L. Lan, P. Xiao, Z. Lin, S. Sun, W. Song, E. Song, P. Gao, P. Zhang and J. Peng, *J. Mater. Chem. C*, 2016, **4**, 2072.
22 S. Sun, L. Lan, P. Xiao, Z. Lin, H. Xu, M. Xu and J. Peng, *RSC Adv.*, 2015, **5**, 15695.
23 J. Veres, S. Ogier and G. Lloyd, *Chem. Mater.*, 2004, **16**, 4543.
24 X. Cheng, M. Caironi, Y. Y. Noh, J. Wang, C. Newman, H. Yan, A. Facchetti and H. Sirringhaus, *Chem. Mater.*, 2010, **22**, 1559.
25 J. Veres, S. D. Ogier, S. W. Leeming, D. C. Cupertino and S. MohialdinKhaffaf, *Adv. Funct. Mater.*, 2003, **13**, 199.
26 D. K. Owens and R. C. Wendt, *J. Appl. Polym. Sci.*, 1969, **13**, 1741.
27 F. M. Fowkes, *J. Phys. Chem.*, 1963, **67**, 2538.
28 B. Singh, P. Senkarabacak, N. S. Sariciftci, A. Tanda, C. Lackner, R. Hagelauer and G. Horowitz, *Appl. Phys. Lett.*, 2006, **89**, 033512.
29 M. J. An, H. S. Seo, Y. Zhang, J. D. Oh and J. H. Choi, *Appl. Phys. Lett.*, 2010, **97**, 023506.
30 J. D. Oh, J. W. Kim, D. K. Kim and J. H. Choi, *Org. Electron.*, 2016, **30**, 131.